PHYSICAL REVIEW D VOLUME 45, NUMBER 1 1 JANUARY 1992

Electromagnetic pulses from high-energy showers: Implications for neutrino detection

E. Zas and F. Halzen
Department of Physics, University of Wisconsin, Madison, Wisconsin 53706

T. Stanev
Bartol Research Institute, University of Delaware, Newark, Delaware 19716
(Received 20 June 1991)

We review the properties of electromagnetic showers in dense media and calculate in detail the associated electromagnetic pulses generated by shower electrons. We perform real-time simulations recording the charge, trajectory, and time of each cascade particle and compute the associated electromagnetic wave. Our results are relevant to experiments detecting radio pulses from showers initiated by cosmic particles interacting with the Earth.

PACS number(s): 96.40.Pq; 29.40.−n; 96.40.Kk; 96.40.Tv

I. INTRODUCTION

Neutrinos can provide information about cosmic sites which are shielded from observation by few hundred grams of matter. Being electrically neutral, they retain directional information on their sources of origin and can thus give a new and complementary view of the Universe. Neutrino astronomy has seen its birth with the observation of the supernova 1979A [1] and is a rapidly developing field [2]. Neutrinos of astrophysically high energy may be produced at compact energetic systems such as x-ray binaries [3] and young supernova remnants [4], in active galactic nuclei [5–7], and in interactions of cosmic rays with gas clouds and interstellar medium [3]. The main background are neutrinos produced in the atmosphere by the decays of mesons created in very-high-energy showers [8]. The expected event rates for astrophysical neutrinos are low and large effective detector volumes are required. Their observation is however important, because it would not only provide very valuable information on their origin and the astrophysical processes involved, but it would also test our understanding of particle physics at energies well beyond existing particle accelerators.

It was nearly 30 years ago that the coherent radio emission from high-energy showers in dense media was proposed as a possible way for detection of high-energy cosmic rays [9]. More recently this old idea has been reconsidered as an alternative possibility for the detection of charged-current interactions induced by superhigh-energy neutrinos [10]. Electrons produced in these interactions develop electromagnetic cascades in the medium. Electromagnetic radiation is emitted by all charged particles in the shower, Čerenkov radiation of visible light is a well-known example. Since the Čerenkov energy spectrum of a fast charged particle rises linearly with frequency, one might conclude that the energy emitted in the low radio frequencies is much smaller than in the optical range. This would make radio emission uninteresting were it not for the fact that the radiation can be emitted coherently by all cascade particles if the wavelength of the emission is large compared with the shower dimensions.

The energy in coherent emission scales with the square of the charge excess in the shower, which is itself linearly proportional to the energy of the incident particle. While the energy in the emission of Čerenkov light is proportional to the energy of the primary particle, the coherent radio emission scales with the square of primary energy. For sufficiently high primary energy the power in radio waves therefore dominates the Čerenkov output in the optical range. It has been claimed that the relatively low cost of electromagnetic pulse detectors may allow a large detection area to be covered with arrays of aerials, providing a cost effective method for detection of neutrino interactions in the energy range above 1 TeV. The technique might also be relevant to the detection of air showers near the Greisen-Zatsepin cutoff.

The radio emission technique has actually been observed in coincidence with air shower arrays produced by high-energy cosmic rays interacting in the atmosphere [11, 12]. Atmospheric instabilities, however, make the systematics very difficult to handle. Antarctic ice provides a natural dense medium for the observation of radio signals. It has very poor absorption coefficient for frequencies below 1 GHz, allowing radio waves to propagate for hundreds of meters before detection. Since the density is much higher than in the atmosphere, the physical dimensions of the showers are much smaller (radiation length is of the order of 36 $g\,cm^{-2}$) and thus the coherence of the radio emission is retained to higher frequencies where more energy is available. The precise threshold for observation of radio signals is very sensitive to the intricate details of the problem, and it is the crucial figure for the feasibility of this neutrino detection technique.

We have used a detailed Monte Carlo simulation that follows the development of the particles to energies well below the MeV range (covering up to 9 orders of magnitude of energy in the development of the cascade), to calculate the intensity of the radio-emission frequency spectrum at different observation angles relative to the incident particle. This is a long and arduous task since the amount of particle tracks is extremely large. We have chosen to study and understand in detail the variations of the relevant quantities both with the incident particle energy and with the unavoidable energy cutoff in the Monte Carlo simulation. For the very energetic showers,

following particles down to the appropriate low-energy threshold is well beyond conventional computing facilities. We will show that it is however possible to obtain the required results by extrapolating achievable Monte Carlo thresholds.

We have divided this article into sections and subsections that simplify identifying discussions of particular interest to the reader. In the next section we discuss shower development and the relevant interactions that lead to the most important features in the showers. Section III is devoted to a classical discussion of the electromagnetic field produced by charged particles in dense media and presents the formulas we have used in a consistent manner. The expected properties of the radiation are discussed. Section IV has all the results of our calculation and compares them to other Monte Carlo shower programs and theoretical results. In Sec. V we discuss the implications of our calculation for neutrino detection. Section VI is devoted to summarizing our main conclusions.

II. ELECTROMAGNETIC SHOWERS

A. Bremsstrahlung and pair production

As an electron or photon passes through matter its energy is degraded by the interactions that take place. For a high-energy electron (photon), bremsstrahlung (pair production) in the fields of the nuclei is by far the hard process with highest cross section. The energy of the primary particle is distributed between the electron and a secondary photon (an electron-positron pair) which will in turn interact producing more secondary particles. As further matter is traversed the energy carried by the primary particle is shared by more and more secondaries which roughly retain the initial particle direction and constitute an electromagnetic cascade shower. This cascading effect carries on until the secondary electrons reach energies below the so-called critical energy E_c. At this energy other processes become as important and electrons are as likely to rapidly lose all their energy through ionization as to radiate hard photons. The energy is finally absorbed in the material by both ionization and the photoelectric effect.

This very simple description of the shower can be made quantitative by noting that both pair production and bremsstrahlung interactions are related processes and their cross sections are approximately equal. In a model developed by Heitler [13], electrons, positrons, and photons are treated equally, transferring half their energy to each of the secondaries at every interaction point. These interactions occur at intervals of $X_0 \ln 2$ where X_0 is the radiation length of the material until the critical energy is reached. (X_0 is the depth of absorber over which the electron attenuates to $1/e$ of its initial energy). Although it oversimplifies all the complicated dynamics, this model works surprisingly well at describing the longitudinal development of the shower having a maximum at $n \simeq \ln(E_0/E_c)$ radiation lengths. The longitudinal scale of the shower is determined by the radiation length of the material and only depends logarithmically on the initial particle energy.

B. Corrections to bremsstrahlung and pair production

The interaction distance relevant in the bremsstrahlung and pair production interactions is inversely related to q, the momentum transfer exchanged with the nucleus. At sufficiently large energy the secondaries are nearly collinear and hence the interaction region for the process $r_{\rm int} \simeq 1/q$ can be approximated by

$$r_{\rm int} \sim \frac{2E}{m_e^2} \begin{cases} (1-x)/x, & \text{for bremsstrahlung;} \\ x(1-x), & \text{for pair production.} \end{cases} \quad (1)$$

Here x represents the fraction of energy given to the photon (electron) in bremsstrahlung (pair production).

The important point is that the effective interaction distance *increases* with larger incident particle energy [14]. For low energies when the interaction distance is much less than the atomic radius, the Coulomb field of the nucleus is just that of the nucleus, a point charge of charge Z (no screening is to be considered). For higher energies, as the interaction distance increases to be comparable to the atomic size, corrections due to electron screening of the nuclear field have to be taken into account (this regime is usually referred to as the intermediate screening region). At high enough energies it becomes much larger than the atomic radius and hence screening is maximum (full screening). There are elaborate analytic shower models making simplifying assumptions, usually referred to as approximations A and B [15]. These models solve the diffusion equations for the shower development using the expression for the complete screening approximation.

At even higher energies the interaction distance grows to become of the order of the typical separation of the atoms. At such energies the screened fields of *all* the nuclei in the nearby region have to be considered. The Landau-Pomeranchuk-Migdal [16, 17] (LPM) effect is caused by the collective atomic potential of the material. The effect is very sensitive to the density of the absorber since the crucial parameter is the mean atomic separation; it has two main implications.

(i) For incident particle energies (E_0) above a certain value ($E_{\rm LPM}$) which depends on the density of the medium, the total cross sections for both processes are dramatically reduced. In the high-energy limit, the full-screening pair production (bremsstrahlung) cross section tends to a constant (increases logarithmically). When the LPM effect is considered both cross sections fall instead as $\sqrt{E_0}$ above $E_{\rm LPM}$. In Heitler's simple picture this implies that as long as the particles in the shower have energies above $E_{\rm LPM}$ the interactions would occur at intervals larger than the radiation length by an approximate factor $\sqrt{E/E_{\rm LPM}}$. The first few interactions are modified in this way but once the energy of the shower particles becomes less than $E_{\rm LPM}$, the previously described longitudinal structure is reobtained. The LPM effect should only affect the early stages of the shower development.

$E_{\rm LPM}$ has been estimated [31] at $61.5X_0$ TeV, where X_0 is in cm; (ii) for bremsstrahlung, the effective interaction distance also becomes larger than the separation between nuclei when the fraction of energy transferred to the photon becomes very low, see Eq. (1). The interference between different nuclei also has the effect of reducing the cross section for the emission of soft photons; it, in fact, eliminates the infrared "catastrophe" associated with them by providing an effective low photon-energy cutoff for the bremsstrahlung cross section. The cutoff takes place at a fixed fraction of the incident energy which is different for each medium. This is also a drastic effect; moreover, it should be observable at energies well below $E_{\rm LPM}$. Nonetheless it is expected to have little effect on the shower development because the majority of the soft photons in a high-energy shower are mostly produced by low-energy electrons and positrons; they vastly outnumber those produced by high-energy electrons. If the LPM effect is "switched off," the fraction of "unphysical" low-energy photons (below the cutoff) produced by the high-energy electrons is insignificant.

C. Multiple elastic scattering

Interactions with nuclei are also responsible for the main features of the transverse structure of the electromagnetic showers, although in this case it is elastic (Rutherford) scattering. Because of the well-known $\sin^{-4}\theta$ behavior for the differential cross section, the combination of multiple scattering at low scattering angles clearly dominates the processes of single large-angle scattering. The theory of multiple scattering has been studied long ago under a number of different approximations yielding fairly equivalent results [18–21]. Molière's theory uses the screened atomic potentials in his formalism which is the most commonly used. An adequate approximation to the distribution can be obtained by retaining the first two terms in his Bessel function expansion. The mean deflection angle for an electron of energy E traversing a depth t measured in radiation lengths is given approximately by the first term which is a Gaussian of width [18]

$$\theta_{\rm MS} \simeq \frac{E_{\rm MS}}{E}\sqrt{t}\,, \tag{2}$$

where

$$E_{\rm MS} = m_e\sqrt{\frac{4\pi}{\alpha}} \simeq 21\ {\rm MeV}\,. \tag{3}$$

While all the interactions contribute to the transverse spread of the particles, the mean angle of multiple scattering dominates (except for extremely thin foils) because of the large number of elastic interactions. There are analytical three-dimensional theories that take into account multiple elastic scattering both using Molière's theory and in the Fokker-Planck approximation. A convenient transverse scale of the shower is the Molière radius which, in radiation length units, is given by the ratio $E_{\rm MS}/E_c$.

D. Interactions with atomic electrons

The interactions mentioned so far would not cause any charge asymmetry in the shower. This description is still not sufficiently accurate since the interactions of each shower particle with the atomic electrons contributes to an overall negative charge excess. This asymmetry largely enhances the low-frequency region of the Čerenkov spectrum as will be explained in the following section and it is thus crucial in the understanding of the coherent radioemission from electromagnetic cascade showers.

The main interaction of shower photons with atomic electrons is Compton scattering ($\gamma + e^-_{\rm atom} \rightarrow \gamma + e^-$) which incorporates atomic electrons to the shower. It is the main mechanism for creation of the excess negative charge mainly because the number of photons in a shower is larger than the number of positrons. Photons interact also via the photoelectric effect although in this process atomic electrons are not accelerated into the shower and thus this mechanism does not contribute to the excess charge in the shower. The photoelectric effect is however very important since it becomes the dominant cross section at low enough energies and thus it is responsible for ultimately terminating the photons in the cascade shower.

Shower positrons interact with atomic electrons both via Bhabha scattering ($e^+ + e^-_{\rm atom} \rightarrow e^+ + e^-$) and via annihilation in flight ($e^+ + e^-_{\rm atom} \rightarrow \gamma\gamma$). While annihilation only contributes to the excess charge by terminating positron trajectories, Bhabha scattering contributes by adding electrons to the shower and reducing the energy of the incident positron. Lastly, the shower electrons interact with atomic electrons via Møller scattering ($e^- + e^-_{\rm atom} \rightarrow e^- + e^-$). This process also incorporates electrons to the shower although it does not modify the total energy carried by electrons in the shower.

The cross sections for both Bhabha and Møller scattering are infrared divergent; i.e., they are singular when the momentum fraction of either of the secondary particles, x and $(1-x)$, tends to zero. Therefore, the effect of multiple scattering with production of low-energetic secondaries has to be integrated out and treated as a continuous energy loss. This is completely analogous to the interpretation of the divergent part of the bremsstrahlung cross section as a continuous loss. Ionization losses are defined as the sum of all of these continuous losses. The precise definition is somewhat blurred because of the arbitrarity in the cutoff parameters for the regularization. In this language the ionization losses of Bhabha and Møller origin contribute to the excess charge in the shower too.

III. ELECTROMAGNETIC RADIATION

A. Radiation from accelerated charges

It is well known that an accelerated charge radiates electromagnetic waves. In a dielectric medium the particles also radiate because the medium responds coherently to the passage of a charged particle. For linear, homogeneous, and isotropic media, induced current and polar-

ization effects are automatically considered by the fields $\mathbf{D} = \epsilon_r\epsilon_0\mathbf{E}$ and $\mathbf{H} = (\mu_r\mu_0)^{-1}\mathbf{B}$ where μ_r (μ_0) and ϵ_r (ϵ_0) are, respectively, the relative (free space) permeability and permittivity. The wave equations for these fields have a smaller wave velocity. The ratio of the speed of light in a vacuum to that in the medium is given by the refractive index $n = \sqrt{\epsilon_r\mu_r}$.

Using the standard Liénard-Wiechert retarded potentials, the electric and magnetic fields are shown to have two components: the so called "near field" and the "radiation field." At every space-time point $x = [x^0, \mathbf{x}]$, they correspond to the two terms in

$$\mathbf{E}(t,\mathbf{x}) = \frac{e\mu_r}{4\pi\epsilon_0}\left[\frac{\mathbf{u}-n\boldsymbol{\beta}}{\gamma^2|1-n\mathbf{u}\cdot\boldsymbol{\beta}|^3R^2}\right]_{\text{ret}} + \frac{e\mu_r}{4\pi\epsilon_0 c}\left[\frac{\mathbf{u}\times[(\mathbf{u}-n\boldsymbol{\beta})\times\dot{\boldsymbol{\beta}}]}{|1-n\mathbf{u}\cdot\boldsymbol{\beta}|^3R}\right]_{\text{ret}}, \tag{4}$$

$$\mathbf{H}(t,\mathbf{x}) = \sqrt{\frac{\epsilon_r\epsilon_0}{\mu_r\mu_0}}\,[\mathbf{u}]_{\text{ret}}\times\mathbf{E}(t,\mathbf{x}). \tag{5}$$

Here $\boldsymbol{\beta}$ is the particle velocity in units of c and $\mathbf{u}$ is a unit vector in the direction of the observation point from the particle position. The subscript ret refers to all the quantities within the square brackets which have to be evaluated at an instant τ defined by the condition $(x^0 - r^0)^2 - n^2|\mathbf{x}-\mathbf{r}(\tau)|^2 = 0$, i.e., the "light-cone condition." In the rest frame of the observer the retarded time t_r is simply related to the observation time x^0 by

$$\frac{x^0 - ct_r}{n} = |\mathbf{x}-\mathbf{r}(\tau)| = R. \tag{6}$$

The fields at an instant $t = x^0/c$ depend on the particle trajectory at an instant t_r such that a light signal from $\mathbf{r}(t_r)$ arrives at point $\mathbf{x}$ at the required time t. R is the (retarded) distance from the point in the particle trajectory when the radiation was emitted to the observation point (hence the name retarded potentials).

The two terms in Eqs. (4) differ in the power of R by which they are suppressed. The first term falls like R^{-2} corresponding to the Lorentz-boosted static Coulomb field. Energy deposition, if any, only happens in the surroundings of the particle and there is no wave associated with it. The second term corresponds to the radiation field; both the electric and magnetic fields fall as R^{-1}, which implies that the energy flux falls like R^{-2} as corresponds to an outgoing spherical wave front.

Noting that the angular velocity of the particle with respect to the observation point is clearly given by $R\,d\boldsymbol{\theta}/dx^0 = \mathbf{u}\times\boldsymbol{\beta}$ and that the relation between observation and apparent time intervals as seen at the observation point is $d(ct_r) = (1-n\mathbf{u}\cdot\boldsymbol{\beta})dx^0$, it is a simple exercise to show that the radiation term is exactly proportional to the apparent angular acceleration of the charge. The corresponding expression is [11, 22, 23]

$$\mathbf{E}(t,\mathbf{x}) = \text{sgn}\,[1-n\mathbf{u}\cdot\boldsymbol{\beta}]\;\frac{e}{4\pi\epsilon_0c^2}\mathbf{u}\times\frac{d^2\boldsymbol{\theta}}{dt_r^2}. \tag{7}$$

This expression is often referred in the literature as "Feynman's formula" and has been used as a means of Monte Carlo evaluation of electromagnetic pulses generated by air showers [24, 25].

B. Frequency spectrum, Čerenkov radiation

For the purpose of calculating the pulse generated by showers it turns out to be most convenient to work with the frequency Fourier transforms of the electromagnetic fields. We define the frequency Fourier transform of the electric field as

$$\mathbf{E}(\omega,\mathbf{x}) = 2\int dt\, e^{i\omega t}\mathbf{E}(t,\mathbf{x}). \tag{8}$$

Using this definition for the Fourier components of the electric field and the orthogonality condition in Eq. (5) for the magnetic field, the power radiated per solid angle in a given direction from the particle trajectory is clearly given by the following integral over the frequency [$\nu = \omega/(2\pi)$] spectrum:

$$\frac{dW}{d\Omega} = \frac{1}{4}\sqrt{\frac{\epsilon_r\epsilon_0}{\mu_r\mu_0}}\int_{-\infty}^{\infty}d\nu\,|R\mathbf{E}(\omega,\mathbf{x})|^2 = \frac{1}{2}\sqrt{\frac{\epsilon_r\epsilon_0}{\mu_r\mu_0}}\int_0^{\infty}d\nu\,|R\mathbf{E}(\omega,\mathbf{x})|^2. \tag{9}$$

The last equality here corresponds to the physical case of $\mathbf{E}(t,\mathbf{x})$ being a real function so that the negative-frequency part of the integral contributes as much as the positive frequency. Performing the Fourier integration of the radiation term in Eq. (4) (at large distances only the radiated fields are relevant) in the apparent time variable, it displays a simple and intuitive form:

$$\mathbf{E}(\omega,\mathbf{x}) = \frac{e\mu_r}{2\pi\epsilon_0c^2}i\omega\int dt_r\, c\boldsymbol{\beta}_\perp\,\frac{e^{i\omega[t_r+R(t_r)/c]}}{R(t_r)}, \tag{10}$$

where R is the distance from the particle to the observation point. In fact this result can be obtained directly solving the inhomogeneous Maxwell's equations in the transverse gauge. The standard convolution of the transverse current with the appropriate Green's function gives the solution

$$\mathbf{E}(\omega,\mathbf{x}) = \frac{e\mu_r}{2\pi\epsilon_0c^2}i\omega\int\int\int\int dt'\,d^3\mathbf{x}'\times e^{i\omega t'+i|\mathbf{k}||\mathbf{x}-\mathbf{x}'|}\frac{\mathbf{J}_\perp(t',\mathbf{x}')}{|\mathbf{x}-\mathbf{x}'|}, \tag{11}$$

which gives Eq. (10) for a point charge current. Here $|\mathbf{k}| = k = n\omega/c$ and $\mathbf{J}_\perp$ is a divergenceless component of the current whose Fourier components are transverse to the direction of observation, $\mathcal{J}_\perp(\omega,\mathbf{k}) = \mathbf{u}\times[\mathbf{u}\times\mathcal{J}(\omega,\mathbf{k})]$.

The integrals on the right-hand side of Eqs. (10) and (11) resemble the Fourier component of the current density. In the large-R limit they are precisely the Fourier transforms of the transverse current density (its projection perpendicular to the line of sight), up to a constant phase factor and an overall factor R^{-1}. Indeed

if $R = |\mathbf{x} - \mathbf{x}'|$ is large, it can be considered constant over the particle trajectory and the phase factor $i|\mathbf{k}||\mathbf{x} - \mathbf{x}'| \simeq ikR - i\mathbf{k} \cdot \boldsymbol{\rho}(\tau)$, where $\boldsymbol{\rho}(\tau)$ gives the position vector of the particle with respect to $\mathbf{x}$.

It is then straightforward to show that a charged particle moving uniformly between two fixed points corresponding to subscripts 1 and 2 produces an electric field with frequency Fourier transform given by the expression

$$\mathbf{E}(\omega, \mathbf{x}) = \frac{e\mu_r i\omega}{2\pi\epsilon_0 c^2} \frac{e^{ikR}}{R} e^{i(\omega - \mathbf{k}\cdot\mathbf{v})t_1} \mathbf{v}_\perp \left[\frac{e^{i(\omega - \mathbf{k}\cdot\mathbf{v})\delta t} - 1}{i(\omega - \mathbf{k}\cdot\mathbf{v})}\right], \tag{12}$$

where $\mathbf{v}$ is the particle velocity and δt is the time interval between the end points of the track. It is worth remarking that in a dielectric medium the modulus of the wave vector is related to the frequency $|\mathbf{k}| = \omega/c'$, c' being the speed of light in the medium. If the particle velocity is greater than the speed of light then $\omega - \mathbf{k}\cdot\mathbf{v} = \omega(1 - n\boldsymbol{\beta}\cdot\mathbf{u}) = 0$ at the Čerenkov angle, $\cos\theta_C = (n\beta)^{-1}$.

Up to an overall phase factor the term in the square brackets in Eq. (12) is simply $\delta t \sin y/y$ where $y = \pi\nu\delta t(1 - n\beta\cos\theta)$. It thus resembles the familiar diffraction pattern of light by a slit. By expanding $\cos\theta$ around the Čerenkov angle, the angular distribution of the Fourier components of the electric field should exhibit such a pattern around the Čerenkov angle. The first zeros of the diffraction pattern happen at $\delta\theta \simeq \left[\nu\,\delta t\sqrt{n^2\beta^2 - 1}\right]^{-1}$. In the limit of $y \to 0$ (either for low frequencies or for observation angles very close to the Čerenkov angle) Eq. (12) reduces to [11]

$$R\mathbf{E}(\omega, \mathbf{x}) = \frac{e\mu_r i\omega}{2\pi\epsilon_0 c^2} \mathbf{v}_\perp\, \delta t\, e^{i(\omega t_1 - \mathbf{k}\mathbf{r}_1)} e^{ikR}. \tag{13}$$

The electric-field amplitude is proportional to the track length perpendicular to the line of sight $l_\perp = |\mathbf{v}_\perp|\delta t$ and to the angular frequency ω. This approximation works at the Čerenkov angle for all frequencies and at sufficiently low frequencies for all angles. The meaning of "sufficiently" here is dependent on the time difference between the track end points, δt. For an infinite track the time lag between signals at the end points is also infinite and the approximation only works at the Čerenkov angle; moreover, as the observation angle departs from its Čerenkov value, interference between different parts of the track are destructive and the radiation is sharply collimated *at all frequencies*. For a finite particle track length, however, collimation effects around the Čerenkov angle disappear when $y \ll 1$ or $\nu\delta t(1+n) \ll 1$. Moreover for a finite particle track there is also some radio emission below the Čerenkov particle energy threshold given by $n\beta_{\rm th} = 1$. All these finite track effects are correctly taken into account through Eq. (12).

Equation (12) is a useful expression that helps us understand the behavior of Čerenkov radiation as the frequency is varied. Substituting it into the total power emitted in Eq. (9) and in the limit of an infinite particle track $\delta t \to \infty$, we can replace the square of the square brackets in Eq. (12) by a δ function at the Čerenkov angle. The angular integration reproduces the well-known Frank-Tamm result [26]

$$\frac{d^2W}{d\nu\, dl} = \left(\frac{4\pi^2\hbar}{c}\alpha\right) z^2\nu \left[1 - \frac{1}{\beta^2 n^2}\right], \tag{14}$$

where $dl = c\beta\delta t$ is the track length of the charged particle.

C. Electric field due to all shower particles

In an electromagnetic shower there are contributions to $\mathbf{E}(\omega, \mathbf{x})$ from all the charged-particle tracks. Therefore, for the frequency components with wavelengths much larger than the dimensions of the shower, the emission from all the particles is coherent and the approximation of Eq. (13) holds. It is clear that the electric field is proportional to the sum of the track lengths perpendicular to the line of sight and that electrons and positrons contribute with opposite signs. It is therefore the excess charge in the shower that is responsible for the electric field. For an estimate of the power radiated we could consider the whole shower as a large charge (the excess charge) traveling through a medium over an average distance (average track length). This approximation has been used to estimate the properties of coherent radiation from electromagnetic showers in ice [10].

As we consider higher-frequency components of the radiation it is clear that Eq. (13) breaks down and the interference effects between each track length are not as simple as a sign change between positrons and electrons. The exponent in the square brackets of Eq. (12) may be offset from zero in several ways. The observation angle offsets the exponent through the geometrical path-time difference of the two end points of the track, Δt. Even at the Čerenkov angle the exponent is not quite zero because of the angular deviation of each particle track from the shower axis; departures of observation angle from the critical value will destabilize coherence. As the frequency increases destructive interference sets in for a fixed observation angle. Particle time delays as well as the subluminal velocities of the particles also contribute to the offset of coherence.

The complicated behavior can be better understood considering three different regimes as regards the interference between the radiation of all the particles in the shower. In the completely incoherent regime the wavelength of the radiation is much smaller than the size of the particle tracks; all the geometrical distances between particles as well as the particle time delays give a random phase to the radiation. The powers contributed by each particle track add up incoherently. This corresponds to the well-studied optical Čerenkov emission on which Čerenkov air telescopes are founded. In this regime the amount of radiation emitted by each track is proportional to the length of the track and is confined to the portion of the Čerenkov cone spanned by the individual tracks. Electrons and positrons contribute to the power with equal signs, the total power is proportional to the sum of the track lengths of all electrons and positrons. We shall

refer to this sum as the "total track length." The "total projected track length" is analogously defined as the sum of the individual track lengths *projected* onto the shower axis.

In the low-frequency extreme of the spectrum the coherence is *full*; every wavelet is emitted in phase throughout the spacetime points in the shower development. The wavelength of the radiation must be much larger than the shower dimensions and the typical time delays for each particle multiplied by the wave velocity. In this limit only the excess number of electrons in the shower matters. The electric field vector contributed by each particle is proportional to the track length associated with the excess charge projected onto the plane perpendicular to the line of sight according to Feynman's formula. Positive and negative charges contribute with opposite sign. We define the "weighted projected track sum" as the difference of the track lengths due to electrons minus those due to positrons, after projecting them onto the shower axis. This is the projected track length associated with the excess charge in the shower and it is the relevant quantity in the calculation of the electric field as observed in the direction perpendicular to the shower axis.

In between these two regimes there is a region of partially coherent effects in the space of frequency and observation angle. When the observation angle is close to the Čerenkov angle full coherence is retained to higher frequencies since particles traveling at nearly the speed of light emit radiation in phase at this angle. Full coherence is however lost because of the lateral separation between particle tracks of the modified directions of individual velocities, and because of the geometric and kinematical delays of each particle. We can expect a Čerenkov peak around the Čerenkov angle of narrower width as the frequency is increased, until the coherence is completely lost. Clearly the complication of the problem forbids an analytical calculation without a large amount of simplifying assumptions. The details of this region are however crucial for the determination of thresholds for detection of showers on the basis of the coherent radio pulse they generate.

IV. NUMERICAL CALCULATION

The Monte Carlo program developed for this calculation is based on standard routines developed by Stanev and Vankov [27] as well as for EGS4 [28]. All the results shown in this article have been made for showers developed in ice, since it has been suggested to use the South Pole ice cap as a massive high-energy neutrino detector [10]. The results are however not expected to deviate significantly for dense homogeneous media of low atomic weight. The radiation length used is $X_0 = 36.08\ \mathrm{g\,cm^{-2}}$ which is very similar to that of air. Although most of the general discussion of this article still applies for the calculation of the electromagnetic pulses in air showers, the actual numerical calculation requires a radically different approach and has been addressed elsewhere. If the atmosphere were uniform in density we would expect the shower dimensions to scale pretty accurately with the ratio of the ice density ($\rho_{\mathrm{ice}} = 0.924\ \mathrm{g\,cm^{-3}}$) to that of air, i.e., by a factor of order 1000. The coherent nature of the electromagnetic pulse generated thus changes in a substantial way. Since the shower dimensions are comparable to typical observation distances, different approximations have to be made. Moreover the calculation is relevant for cosmic-ray observations rather than for neutrino astrophysics thus justifying a separate discussion.

When discussing the frequency spectrum of the electric field we shall consider frequencies well above 1 GHz for the purely academic purpose of comparison with theoretical expectations and better understanding of the mechanisms involved. Above such frequencies the absorption coefficient for electromagnetic waves (microwaves) in ice becomes non-negligible and the permittivity of the medium has a rich structure that modifies the electromagnetic pulse spectrum in a substantial way which depends on the properties of the ice and on the distance from the observation point to the cascade. We shall not address this issue here.

A. Monte Carlo details

We have developed a fast Monte Carlo program attempting to take all previously described effects into consideration to reproduce the features of the radiation for the different frequencies in the fully coherent and partially coherent regimes. The aim has been to introduce all features that are thought relevant to the problem without spurious complicated calculations that would slow the time of execution and thus limit dramatically the maximum incident particle energies that could be considered. With this in mind we have calculated the cross sections for bremsstrahlung and pair production taking the LPM effect into account both in the total cross section as well as in the distributions for the fractions of energy of the secondaries. We have also included low-energy corrections for these processes according to Koch and Motz [29]. When necessary, the results have been parametrized to give sufficiently accurate results for our purposes. Interactions with atomic electrons are carefully put in for Compton, Bhabha, and Møller scattering as well as for positron annihilation in flight. Multiple scattering is implemented according to Molière's theory retaining the first two terms in his expansion, and, lastly, ionization losses for electrons and positrons have been included.

We have neglected the photoelectric effect which should become significant in ice only for kinetic energies well below 100 keV [30]. As will become clear from the discussions in Secs. IV C and IV D, particles below about 100 keV (which happens to coincide with the Čerenkov threshold for radio waves in ice, 106.6 keV) are not expected to contribute much to the electromagnetic pulse generation. The omission is thus completely justified.

Particular care was taken in keeping close track of timing for each individual particle in the shower. Delays are measured with respect to an ideal particle moving along the shower axis at the speed of light. There are two main sources of delays: part of the delay is associated with the

particle velocities being smaller than c, while the remaining delays are purely geometrical and arise because the shower particles deviate from the direction of the shower axis. Approximate account was taken of the time lag associated with multiple scattering. This was accomplished by averaging over direction cosines at the end points of the subsegments of the tracks as split in the Monte Carlo for multiple scattering and ionization-loss calculations. The maximum subsegment length is a small fraction of the radiation length at high energies, and as the particle velocity is small it is worked out by splitting a crude estimate of the particle range in several subsegments.

In the calculation of the electromagnetic pulse we have made extensive use of Eq. (12), keeping the relative phase factor for each particle that corresponds to its time delay and geometrical position at the start point of the track. In order to make use of this equation particle tracks were approximated by straight lines between the end points and the velocity assumed constant. We consider two end points to each track corresponding to the point at which the particle is created and an end point arbitrarily defined when the particle reaches a Monte Carlo threshold energy $E_{\rm th}$. At the end point the particle is assumed to be instantaneously absorbed and radiation emitted in the absorption is neglected for the radiation pattern calculation. The time delay δt for each track is then the geometrical apparent time difference associated with the space-time end points which depends on the direction of observation.

B. Shower structure: comparison with other calculations

As a means of checking our simulation and for the purpose of comparison with other simulations of electromagnetic showers, we briefly discuss the results for both the longitudinal and transverse shower structure. We will contrast them to established analytical approximations. As a spinoff we will obtain differences in the depth distribution due to the LPM effects as well as differences in the lateral structure due to the effect of atomic interactions and nonconstant energy losses for electrons and positrons. These effects are neglected in some of the approximations with which we compare our results. This discussion will be helpful for understanding the complex structure of the radiation pattern from showers generated by high-energy particles interacting with matter.

Figures 1 and 2 show the longitudinal development of the shower and it is compared to the results obtained under Approximation B [15] of linear shower theory, which solves approximate diffusion equations for the shower with the full screening versions of the pair production and bremsstrahlung cross sections and a constant term for energy loss due to ionization. The results of the Monte Carlo simulation are very close to the analytic calculation for initial particle energies below 100 TeV. For showers of primary energies of 1 PeV,[1] there are observable differences with the analytic results plotted (Fig. 2). There is a slight normalization difference which can be related to the fact that we have imposed an artificial threshold in the Monte Carlo simulation. The threshold effect is shown for showers of $E_0 = 100$ TeV and 1 PeV. The difference in shape between the Monte Carlo and approximation-B distributions is due to the LPM effect. There is a shift in position of the maximum as well as a broadening of the depth distributions. For 1-PeV showers there is only a hint of an effect which becomes clearly patent as the primary energy is increased to 10 PeV, in agreement with previous calculations for water by Stanev

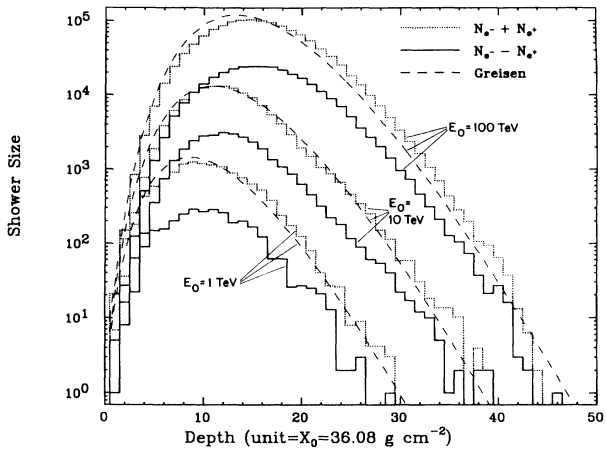

FIG. 1. Depth development of the total number of electrons and positrons and the excess number of electrons for 1-, 10-, and 100-TeV electron-initiated showers. The Monte Carlo threshold energy is 1 MeV. Depth is measured in radiations lengths of ice. The dotted lines are the results in approximation B of shower theory [15] in the limit of $E_{\rm th} \to m_e$.

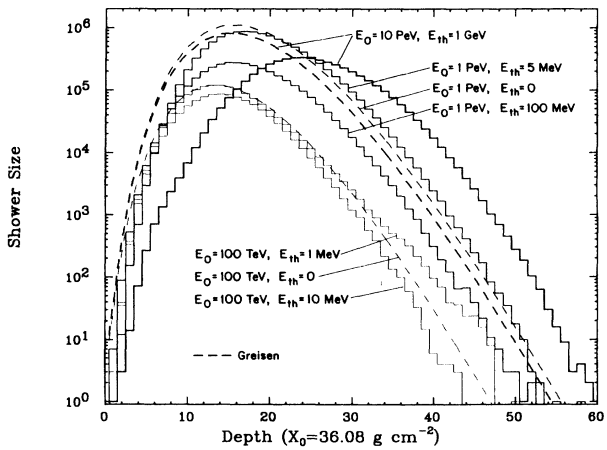

FIG. 2. Depth development of the total number of electrons and positrons for 100-TeV, and 1- and 10-PeV electron showers. Different thresholds are shown for 100-TeV and 1-PeV showers. Depth is measured in radiations lengths of ice. The dashed lines are the results under approximation B. The result of approximation B for a 10-PeV shower is shown for $E_{\rm th} = 1$ GeV (thin dashed line).

[1] 1 PeV is equal to 10^3 TeV= 10^{15} eV.

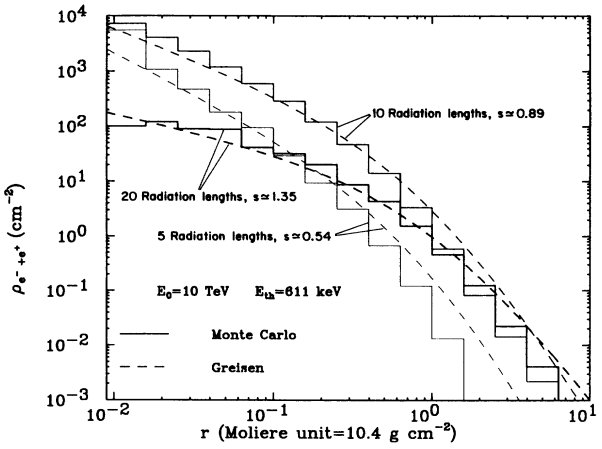

FIG. 3. Lateral electron+positron density for a 10-TeV shower and a kinetic-energy threshold of 100 keV ($E_{\rm th}$ = 611 keV). The radial distributions for three different shower ages s are compared. Dashed lines are Greisen's parametrization.

et al. [31] We have noted that both of these effects seem more pronounced for particle energies around 25 MeV. Both Figs. 1 and 2 give us a good idea of the large statistical significance of the Monte Carlo results for a single shower because of the extremely large number of low-energy particles involved.

The results of the lateral distribution of the shower agree considerably well with the approximate analytic results obtained in the three-dimensional cascade theory in Approximation B. Our results are measured in Molière units as defined in Sec. II C which correspond to 10.4 g cm^{-2} for a critical energy of 73 MeV. We have compared our results with the parametrization from Greisen [33] which is shown in Figs. 3 and 4. Figure 3 gives the electron density distribution for a E_0 = 10-TeV electron shower, and Fig. 4 more conveniently shows the difference between our results and those parametrized by Greisen for a 100-TeV shower.

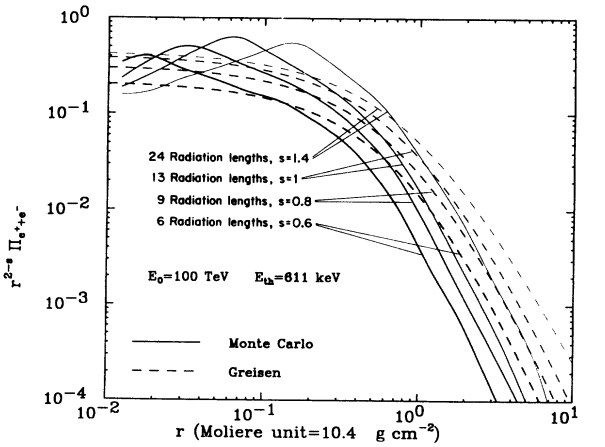

FIG. 4. Lateral electron+positron density for a 100 TeV shower and a threshold of 611 keV. Π is normalized by the condition [14], $\int_0^\infty dr\, 2\pi r \Pi = 1$. The radial distributions for four different shower ages s are compared. Dashed lines are Greisen's parametrization.

C. Track length results

Besides computing the electron and positrons distributions in three spatial dimensions as well as time, the Monte Carlo program also computes the "total track length," the "total projected track length," and the "weighted projected track sum" as defined in Sec. III C.

One of the most difficult choices in the Monte Carlo simulation is selecting the appropriate value for $E_{\rm th}$. Since the range of electrons drops very quickly as their energy is lowered below about 1 MeV, the track length can be expected to stop increasing as the energy threshold $E_{\rm th}$ is lowered. On the other hand we can expect to have to consider threshold energies below 1 MeV because there is an increasing number of particles being created at lower energies and also because interactions with atomic electrons become more relevant at lower energies and thus the charge asymmetry in the shower rises. The delicate competition between these two features which have opposite effects determines the relevant threshold for the Monte Carlo calculation below which particles do not contribute. We have calculated the track lengths as a function of $E_{\rm th}$ in an attempt to address this question. The results (Fig. 5) are shown to scale very accurately with the incident particle energy. Fluctuations in the shower affect it in a minor way and they decrease for cascades of larger energy because the number of particles in the shower gets exceedingly large. More than 50% of the weighted projected track length is due to particles with kinetic energies between 500 keV and about 6 MeV indicating that these particles have to be well accounted for in the Monte Carlo program.

The small relevance of the LPM effect for the calculation of electromagnetic pulses generated by showers

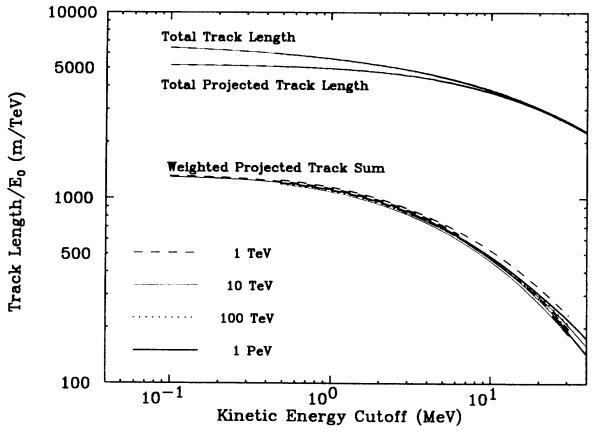

FIG. 5. Shower track lengths for all charged particles in 1-, 10-, and 100-TeV electron showers as a function of the calculational cutoff ($E_{\rm th}$). The three sets of curves correspond to (i) the sum of all track lengths (total track length), (ii) the sum of all track lengths projected onto the shower axis (total projected track length), and (iii) the difference of electron and positron track lengths projected onto the shower axis (weighted projected track sum). Several showers for 1 and 10 TeV primaries are shown to illustrate the effect of fluctuations. The track lengths have been divided by the energy of the primary in TeV to display the scaling features.

can be fully appreciated by considering the shower track lengths for incident particles of large energy. Time limitations force us to choose very high Monte Carlo thresholds for these showers, but the low $E_{\rm th}$ behavior of the curve can be obtained from the lower primary energy results because the lower energy part of the shower should behave in an analogous fashion. Figure 6 shows how even for primary energies of 10 PeV the results for the track length still scale very well, although the LPM effect is clearly shown in the profile of the shower with depth in Fig. 2. The reason is clear since the LPM only affects the shower particles of very high energies, hundreds of TeV, and we know also from Figs. 5 and 6 that the contributions to the track length are due to very-low-energy particles, in the MeV's.

D. Excess charge results

Interactions with atomic electrons cause the shower to develop an excess of electrons over positrons. In order to relate to the electromagnetic pulse calculation we have calculated the charge excess in the shower defined as

$$\Delta q = \frac{N(e^-) - N(e^+)}{N(e^-) + N(e^+)} \,. \tag{15}$$

Figure 7 shows the percentage excess charge in the shower as a function of depth for a threshold energy of 1 MeV and for several incident energies. The excess charge is very sensitive to the threshold in a similar fashion to the track length. The percentage excess charge rises with penetrating depth; when the shower maximum is reached it amounts to $\sim$ 20% and continues rising for further penetration to more than $\sim$ 30% until the shower dies.

We have also addressed the issue of the relative importance of each atomic electron interaction to the charge excess. Figure 8 shows the track lengths as a function of Monte Carlo threshold for four cases corresponding to switching off in the Monte Carlo simulation each one of the four types of interactions with atomic electrons in turn. The calculation was done for 10-TeV showers with a kinetic energy threshold $E_{\rm th}$ = 200 keV. Since the total

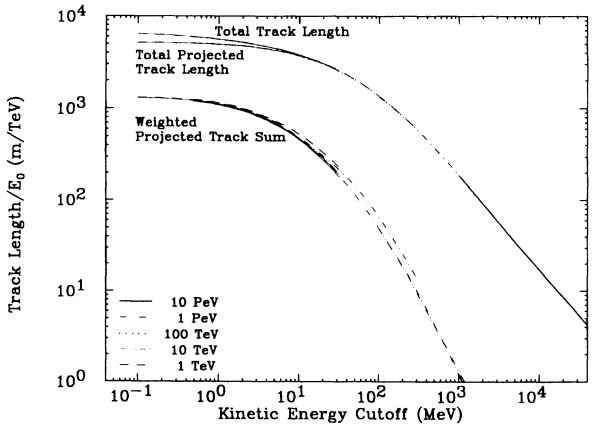

FIG. 6. Same as Fig. 5 including 1- and 10-PeV showers with high thresholds for comparison.

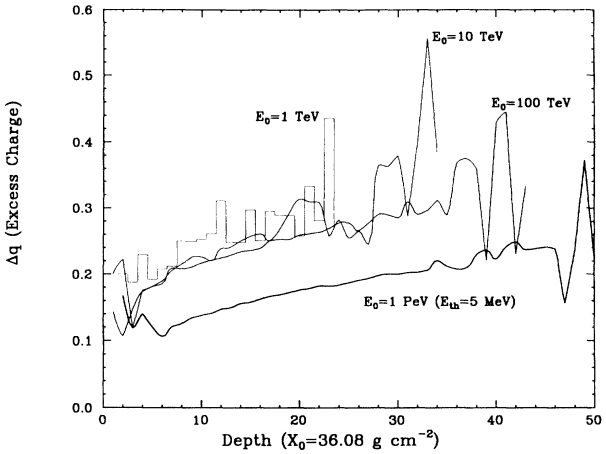

FIG. 7. Depth development of the excess charge as in Eq. (15). The threshold energy is 5 MeV for the 1-PeV shower and 1 MeV for all the others.

track lengths are clearly artificially increased by removing each interaction, we feel the best way of determining the relative role of each interaction is by considering the ratios of the weighted projected track sums to the total projected track lengths. In this way we obtain that the partial contributions of each interaction to the overall excess charge are in decreasing order of importance: (i) Compton scattering ($\sim$ 60%); (ii) Bhabha scattering ($\sim$ 30%); (iii) positron annihilation in flight ($\sim$ 10%); and finally (iv) Møller scattering, which decreases the excess track length ($\sim -5\%$) as it degrades e^- energy. This agrees well with calculations made for air showers [34].

As discussed in Sec. II D the divergence of the cross section for Bhabha and Møller scattering requires that the processes with low-energy secondaries are treated as a continuous energy loss. In the Monte Carlo simulation the threshold naturally regulates the soft divergencies associated with these processes which are dealt by the continuous energy loss formulas. When we remove

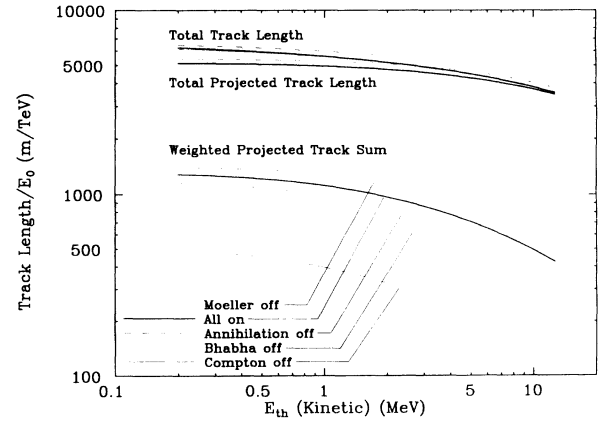

FIG. 8. Same as Fig. 5 for a 10-TeV shower. The effects of artificially removing from the Monte Carlo simulation each of the Compton, Møller, Bhabha, and annihilation cross sections in turn are compared.

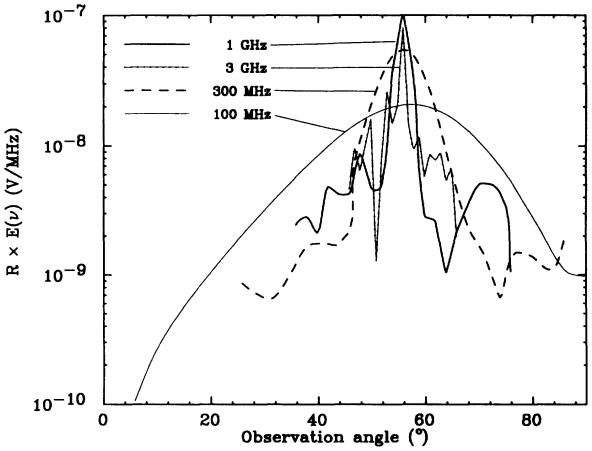

FIG. 9. Angular distribution of the electric field generated by a 1-TeV shower ($E_{\rm th}$ = 611 keV). The observation angle is the polar angle of the radiation with respect to the shower axis. The quantity $RE(\nu)$, distance times Fourier transform of the electric field, is related to power by Eq. (9).

Bhabha or Møller scattering processes from the Monte Carlo simulation we do not change ionization losses. The remaining $\sim$ 5% contribution to weighted track lengths is attributed to the difference in the continuous energy loss between electrons and positrons.

E. Angular distributions of Fourier components of pulse

We have studied in detail the angular distribution and frequency spectrum of the emitted radiation. The calculation has been performed by sampling the contributions to the frequency Fourier transform of the electric field at different frequencies and observation angles. Special care was taken when choosing sampling points so that results show the diffraction patterns characteristic of the problem. The dependence of the calculations on the artificially introduced Monte Carlo thresholds has been studied by comparing results for different thresholds. The differences give us an idea of the expected validity of these results by simultaneously combining Monte Carlo uncertainties as well as uncertainties associated with shower fluctuations.

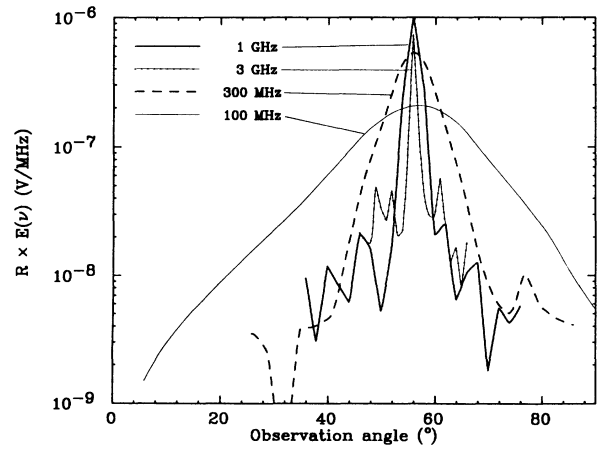

FIG. 10. Same as Fig. 9 for a 10-TeV shower.

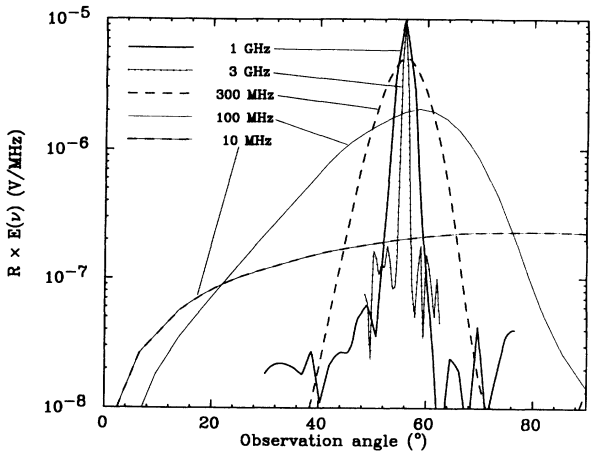

FIG. 11. Same as Fig. 9 for a 100-TeV shower and $E_{\rm th}$ = 1 MeV.

Figures 9–14 show the dependence of the electric field on the observation angle for 1-, 10-, 100-TeV and 1-PeV incident electron energies and clearly display the expected diffraction pattern around the Čerenkov angle. There are several features in these results which are worth remarking. The angular distribution of the signal is pretty uniform for low frequencies showing for an approximate $\sin\theta$ dependence which arises from the projection of the particle tracks on the celestial sphere of the observer. The onset of destructive interference is associated with a peaking effect around the Čerenkov angle which narrows swiftly as the frequency increases. At 1 GHz the Gaussian half-width is of the order of 1.2° about the Čerenkov angle while at the peak of the spectrum, 3 GHz, it narrows to 0.4°. From the analogy with a slit diffraction pattern we expect the width to be inversely proportional to the frequency, a feature that is pretty accurately reflected.

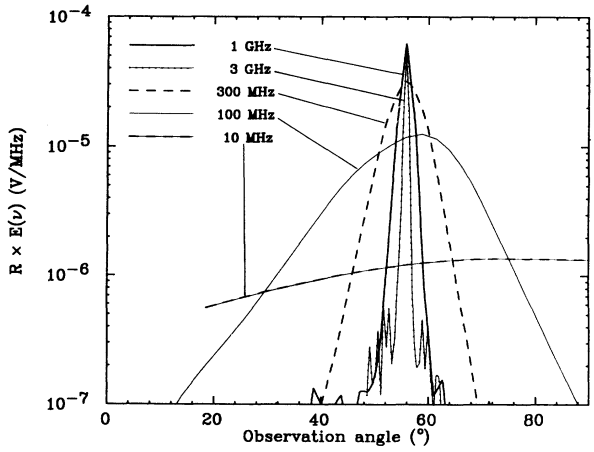

FIG. 12. Same as Fig. 9 for a 1-PeV shower and $E_{\rm th}$ = 5 MeV.

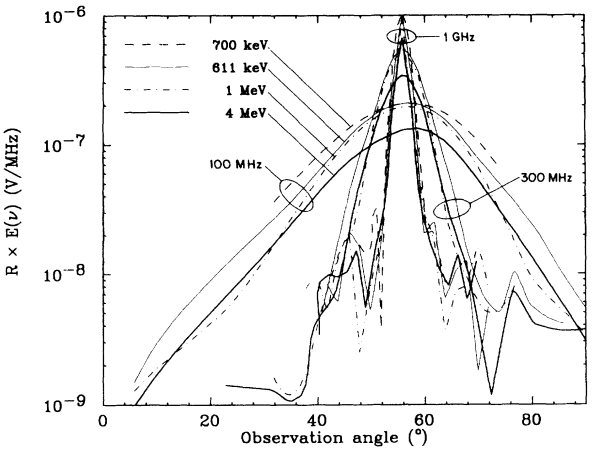

FIG. 13. Same as Fig. 10 for several 10-TeV showers. Calculations with different thresholds are compared.

In Fig. 13 we address the uncertainty in the calculation by plotting the angular distributions of 10-TeV electron showers for four different Monte Carlo thresholds. The results are reassuring since the main features of the Čerenkov peak are clearly unaffected except for a small overall renormalization factor. The differences away from the Čerenkov angle become more significant—they are due to differences in the thresholds and shower fluctuations. While the positions of the secondary and higher order peaks vary slightly, the main features of the diffraction pattern are always present.

Moreover the overall normalization differences agree well with the ratio of the projected track lengths for the different values of $E_{\rm th}$ used, which means that for practical purposes the threshold can be set higher and results corrected for this normalization. This allows for the simulation of pulses generated by very high primary energies if necessary.

In Figs. 14 and 15, we compare the Čerenkov peaks for

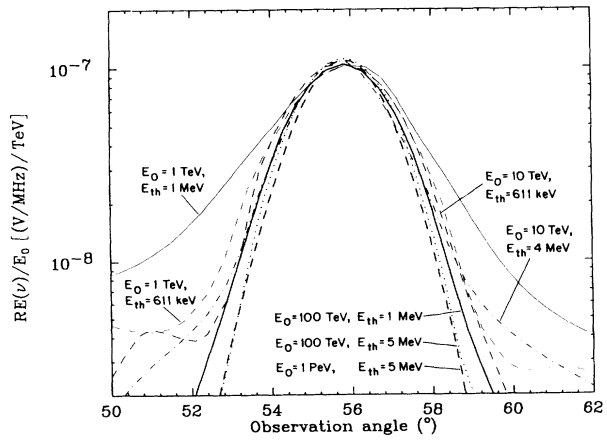

FIG. 14. Scaling properties of the amplitude at the Čerenkov peak at 1 GHz. The peak is shown for 1-, 10-, 100-TeV and 1-PeV showers with different thresholds. Magnitudes of the amplitude have been rescaled according to the threshold used as explained in Sec. IV E.

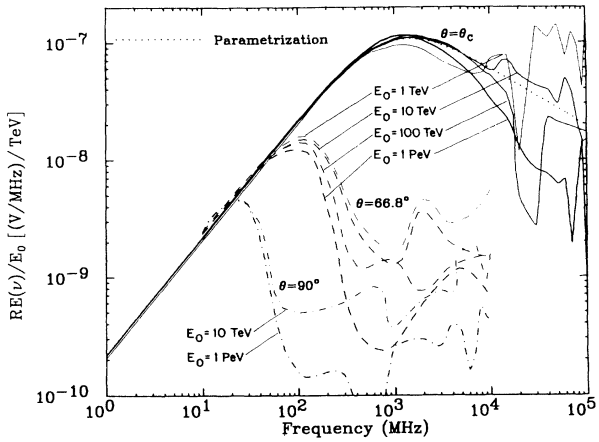

FIG. 15. Frequency spectrum of the electromagnetic pulse. The figure displays 1-, 10-, and 100-TeV showers for different thresholds. The amplitudes have been divided by the energy of the primary in TeV and renormalized according to the threshold. The full curves correspond to observation at the Čerenkov angle (θ_C) to the shower axis. The dashed (dot-dashed) curve corresponds to observation at 66.8° (90°) to the same axis.

different primary energies and different thresholds. We have rescaled our results according to these factors for each different threshold. The calculations then are very consistent and the peak of the radiation is shown to scale very well with energy. It is clear that the angular width of the pulse for a fixed frequency is pretty independent of the primary electron energy at least up to 100 TeV. At 1 PeV the peak is slightly narrower. The effect is small and at least part of it is due to the fact that we have used a slightly higher threshold.

The first minima of the spectra at 1 GHz occur around 5° away from the Čerenkov angle. If we simplify the shower structure as a uniform distribution of point charges traveling at the speed of light over a depth D it can be seen that the minima in the diffraction spectra would be given by the condition

$$D(\cos\theta_C - \cos\theta) = \lambda = \frac{c}{n\nu}. \tag{16}$$

Five degrees away from the Čerenkov angle corresponds to a depth of nearly 6 radiation lengths. We conclude thus that they are mostly reflecting the longitudinal structure of the shower maximum. The shapes of the diffraction patterns are still pretty similar for different primary energies and the magnitude of the electric field at the peak scales accurately with it. The main difference as the primary particle energy is increased is the enhancement of the Čerenkov peak as compared to radiation at other angles. It is clear that this should be so since the electric field should scale with E_0 at the Čerenkov peak but only with $\sqrt{E_0}$ away from it, because the contributions from all the shower particles are no longer coherent.

F. Electromagnetic pulse: Fourier spectrum

Figure 15 (16) shows the magnitude (phase) of the frequency spectrum of the electric field amplitude for obser-

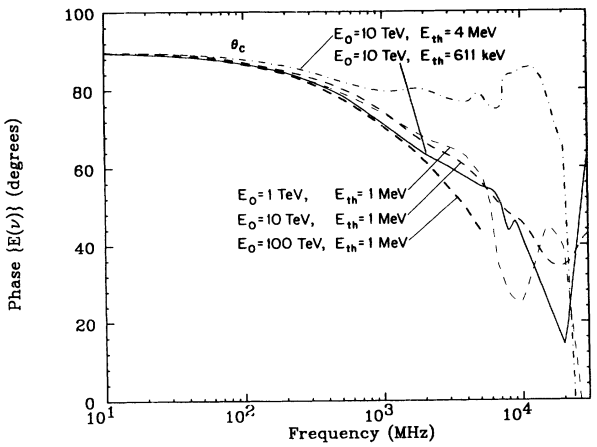

FIG. 16. Phase of the complex Fourier transform of the electromagnetic pulse for 1-, 10-, and 100-TeV showers. The set of curves of 10-TeV showers illustrates the effect of the Monte Carlo threshold on this quantity.

vation at the Čerenkov angle, at 66.8° and at 90° to the shower axis. In Fig. 15 we have superimposed the results for different energies by plotting the ratio of the electric field to the primary energy thus showing the energy scaling features of the calculation. The normalization has been corrected for $E_{\rm th}$ as explained in the previous section. At the Čerenkov angle (55.8°) we observe the departure from linear scaling with energy at around 300 MHz. At 1 GHz the obtained signal is 50% of the expected signal for full coherence using the projected track length as obtained in the program. The spectrum peaks at around 3 GHz and it then dips in the range 10–30 GHz. At these frequencies the features in the spectrum depend more on both $E_{\rm th}$ and primary energy and are subject to larger fluctuations.

The wavelength of the radiation at the peak is of the same order as the Molière radius (11.5 cm). The transverse shower structure causes destructive interference between particles at different positions in the shower front and is the main cause of the onset of decoherence. The position of the peak is in this sense "probing" the transverse shower structure. This explains that the peak is quite independent of the primary energy since the shower lateral spread is known to be pretty insensitive to the initial electron energy too. At higher frequencies the particle delays start to play a more important role and the results become much more sensitive to the threshold. Figure 16 shows how the phase of the field transform also loses reproducibility above 10 GHz, and it shows how the particles below 4 MeV play an important role in the phase above 1 GHz.

The three coherence regions described in Sec. III can be seen from Fig. 15 too. Below 300 MeV the electric field rises linearly with E_0, it corresponds to the fully coherent regime. For an observer whose line of sight forms the Čerenkov angle with the shower axis, the region of partial coherence lies in between 300 MHz and about 10 GHz. The erratic behavior above 10 GHz hints at the onset of the incoherent region in which the field is proportional to $\sqrt{E_0}$. In this region there is still some angular structure but the emission is mostly incoherent. The inner part of the shower or core still contributes coherently but the size of the "coherent disc" reduces as the frequency is raised.

At different observation angles the onset of destructive interference starts at lower frequencies; this is in fact to be expected because away from the Čerenkov angle different stages in the longitudinal development of the shower interfere. Again, assuming a uniform charge distribution along eight radiation lengths, the condition in Eq. (16) would give us a minimum at around 300 GeV for observation at 66.8° and at about 100 GHz for observation at 90°. This is pretty close to what Fig. 15 displays—a sudden cutoff at around these values. Figure 15 may hint at what may be the only modification due to the LPM effect: away from the Čerenkov angle the drop in frequency starts sooner for more energetic showers. According to our simple picture this corresponds to a larger effective shower, i.e., a broader shower maximum which is known to happen because of the LPM effect [31]; see Fig. 2. In the angular distribution of the electric field amplitude it shows as a slight narrowing of the peaks (Fig. 14). If this is the case it may be expected to become more pronounced for 10-PeV showers and above.

G. Practical results

It should be possible to reconstruct the nature of the pulse by undoing the transform using the results of the modulus shown in Figs. 9–15 and the phase in Fig. 16. The cutoff of the spectrum is provided by the absorption properties of the ice, which are well understood. The nice scaling properties of the quantities relevant for pulse calculations allow us to express the results in convenient parametrized form, at least in some regions, which may help simplify further calculations of both reconstruction and transmission of pulses and their detectability, which will not be addressed here.

The track lengths for a kinetic energy threshold of 100 keV are (E_0 in TeV)

$$\text{total track length} = (6423 \pm 1)E_0 \text{ m}, \tag{17}$$

$$\text{total projected track length} = (5174 \pm 3)E_0 \text{ m}, \tag{18}$$

$$\text{weighted projected track sum} = (1300 \pm 10)E_0 \text{ m}. \tag{19}$$

Rough statistical errors are given as an indication of Monte Carlo fluctuations. Approximations made for the cross sections will of course add larger systematic errors.

The results of the electromagnetic spectrum at the Čerenkov angle to the shower axis can be parametrized very well in the region below 1 GHz by the expression

$$R|\mathbf{E}(\omega, R, \theta_C)| = 1.1 \times 10^{-7} \frac{E_0}{1 \text{ TeV}} \frac{\nu}{\nu_0} \frac{1}{1 + 0.4(\nu/\nu_0)^2} \text{ V MHz}^{-1}. \tag{20}$$

Here $\nu_0 \simeq 500$ MHz. We have included our parametrization in Fig. 15, where it can be seen that this expression also works pretty well up to 10 GHz, although the uncertainty and the fluctuations at 10 GHz can vary up to a factor of 2. This part of the spectrum is however starting to get absorbed in ice, and the pulse details should not be very sensitive to this uncertainty in the spectrum.

The angular half-width of the pulse around the Čerenkov angle can be parametrized by a Gaussian peak:

$$E(\omega, R, \theta) = E(\omega, R, \theta_C)\exp\left[-\frac{1}{2}\left(\frac{\theta-\theta_C}{\Delta\theta}\right)^2\right] \quad (21)$$

with $\Delta\theta \simeq 2.4^\circ\ \nu_0/\nu$.

With this simple parametrization the power in the electromagnetic pulse can be calculated using Eq. (9) to be mostly determined by the maximum frequency considered in the spectrum. As an example the energy below 1 GHz is

$$W \simeq 4.5 \times 10^{-14}\left[\frac{E_0}{1\ \text{TeV}}\right]^2 \text{ erg}. \quad (22)$$

We can as a cross-check estimate the power from the excess charge in the shower peaks of the depth distributions of Fig. 1. The excess number of electrons is $\sim 220[E_0\ (\text{TeV})]^2$ electrons over 8 radiation lengths at the shower maximum. According to Eq. (14) the power emitted is thus

$$W \simeq 5 \times 10^{-14}\left[\frac{E_0}{1\ \text{TeV}}\right]^2\left[\frac{\nu_{\max}}{1\ \text{GHz}}\right]^2 \text{ erg}. \quad (23)$$

The agreement is good considering that Eq. (14) does not take into account diffractive effects as well as some destructive interferences between the particles in the shower front. Our estimate of the power is now actually somewhat larger than previous estimates [35], contrary to our previous result in Ref. [36]. The power in the signal is however very sensitive to the upper frequency cutoff which is determined by local absorption. We will avoid power estimates in the threshold calculation of the next section.

V. NEUTRINO DETECTION

The idea of detecting high-energy cosmic rays by looking for the electromagnetic pulse of the showers they produce in dense media is over 30 years old now [9]. It has been recently suggested [10] as a cost-effective means of detecting neutrinos in ice by using the South Pole as a massive detector for upcoming pulses from charged-current interactions of neutrinos that have traversed the Earth from the other side. The low microwave absorption coefficient of ice at low temperatures and its availability at the South Pole made this site, where some experiments have already been performed [35], particularly attractive.

The viability of these experiments is very dependent on the precise conditions of the absorption in the ice and the background noise of the sites, which have to be well measured before accurate calculations of the energy thresholds for neutrino detection are made. We do not want to address further experimental problems such as possible internal reflection of radio signals on the ice-firn-air interfaces or the differentiation of the background from downcoming air showers and other backgrounds which may make this idea impracticable [2].

We can estimate the threshold energy for the electromagnetic shower produced by an electron-neutrino charged-current interaction as a function of distance to the cascade using the results of our calculation. We transform Allan's adapted noise spectrum [11] for a 1-MHz bandwidth receiver to a 1-GHz bandwidth by scaling it down by a factor $\sqrt{1000}$ to account for the bandwidth dependence of both the noise and the pulse amplitude. We shall consider detectable a pulse whose Fourier spectrum at 1 GHz is above the 300-K thermal equivalent as has been suggested by some experiments [37]. This condition would approximately give us the condition of detectability to be [36]

$$E_{\text{th}}\ (\text{PeV}) \simeq 4R\ (\text{km}). \quad (24)$$

The actual neutrino threshold is higher because the average fraction of momentum of the electron in a charged-current interaction is smaller than 1. It has been calculated by Quigg *et al.* [38] to approximately increase logarithmically with incoming (anti)neutrino energy from (0.67 to 0.8) 0.5 to 0.8 in the range of energies $(1$–$10^4]$ TeV. Taking this into account the detection energy threshold at 1 km is close to 5 PeV for both neutrino and antineutrinos. This is a very high threshold. Existing experiments already set limits on high neutrino fluxes which imply extremely low event rates above 5 PeV [39].

These results are order-of-magnitude estimates since they depend critically on the detector parameters. The 300-K noise guess may be improved by parametric amplifiers, arrays of antennas, or helium cooling resulting in a significant reduction of the detector efficiencies for radio-wave quanta. The possibilities of such arrangements are complicated, their cost will certainly be much higher than simple dipole antennas, and they would have to be proven experimentally. We hope however that the efficiency of such arrangements for neutrino detection can be studied in detail with the help of this work.

VI. CONCLUSIONS

We have developed a fast Monte Carlo program to simulate the three-dimensional shower structure induced by ultrahigh-energy particles interacting in a dense homogeneous medium. We have carefully checked our program by comparing our results to other existing calculations and theoretical results. The agreement is good, thus adding to the reliability of our program, although we are not aware of Monte Carlo simulations covering such a large range of energies. We have implemented timing and the capability to calculate all features of the spectrum of the electromagnetic radio pulse generated by such showers.

We have subsequently calculated in detail the spectrum and angular distributions of the electromagnetic

pulses induced by high-energy electron showers in ice. The results show a wealth of information that is of relevance for proposed experiments to detect charged-current neutrino interactions in the ice cap of Antarctica. We have estimated the energy thresholds for incident neutrinos by requiring a signal of equal amplitude to a 300-K equivalent thermal background spectrum corresponding to a 1-GHz bandwidth detector. Our calculation roughly agrees with previous estimates while providing lots of additional information.

Unfortunately our threshold estimate for the neutrino energy is far too high to make this mechanism a cost-efficient detector for the low neutrino fluxes expected at high energies. To sample 1 km in depth, a 5-PeV neutrino is anticipated and the existing limits on high energy neutrinos imply very low event rates unless detectors of area much larger than 1 km^2 are considered.

ACKNOWLEDGMENTS

We are extremely grateful to Charles Goebel for a number of very helpful discussions on classical electrodynamics and Čerenkov emission. This work was supported in part by the University of Wisconsin Research Committee with funds granted by the Wisconsin Alumni Research Foundation, in part by the U.S. Department of Energy under Contract No. DE-AC02-76ER00881, in part by the Texas National Research Laboratory Commission under Grant No. RGFY9173, and in part by the Xunta de Galicia (Spain).

[1] For a review, see, for instance, D.N. Schramm, in *Supernova 1987A, One Year Later; Results and Perspectives in Particle Physics*, Proceedings of the Second Rencontre de la Vallèe d'Aoste, La Thuile, Italy, 1988, edited by M. Greco (Editions Frontières, Gif-sur-Yvette, France, 1988), p. 183; Fermilab Report No. Conf-88/45-A (unpublished).

[2] For a recent review, see, J.G. Learned, in Proceedings of the Second Venice Workshop on Neutrino Telescopes, Venice, Italy, 1990, edited by M. Baldo-Ceolin (unpublished).

[3] V.S. Berezinsky *et al.*, in *Proceedings of the Astrophysics of Cosmic Rays* (Elsevier, New York, 1991).

[4] T.K. Gaisser and T. Stanev, Phys. Rev. Lett. **58**, 1695 (1987).

[5] P.L. Biermann in Proceedings of the Astrophysical Aspects of the Most Energetic Cosmic Rays, Kofu, Japan, 1990 (unpublished).

[6] F.W. Stecker, C. Done, M.H. Salamon, and P. Sommers, Phys. Rev. Lett. **66**, 2997 (1991).

[7] S.W. Barwick *et al.*, presented by F. Halzen, in the Third International Workshop on Neutrino Telescopes, Venice, Italy, 1991 (unpublished).

[8] See, for example, T.K. Gaisser, *Cosmic Rays and Particle Physics* (Cambridge University Press, Cambridge, England, 1990).

[9] G.A. Askar'yan, Zh. Eksp. Teor. Fiz. **41**, 317 (1961) [Sov. Phys. JETP **14**, 441 (1962)].

[10] I.M. Zeleznykh, in *Proceedings of the XXIst International Cosmic Ray Conference*, Adelaide, Australia, 1989, edited by R. Protheroe (Graphic Services, Northfield, South Australia, 1990), Vol. 6, pp. 528–533.

[11] For a good review on cosmic showers and electromagnetic pulses, see H.R. Allan, *Progress in Elementary Particles and Cosmic Ray Physics* (North-Holland, Amsterdam, 1971), Vol. 10, p. 171.

[12] N. Mandolesi, G. Morigi, and G.G.C. Palumbo, J. Phys. A **9**, 815 (1976).

[13] W. Heitler, *The Quantum Theory of Radiation* (Clarendon, Oxford, 1954).

[14] J. Nishimura, in *Handbuch der Physik* Bd. **XLVI/2**, edited by S. Flugge (Springer, Berlin, 1967).

[15] B. Rossi, *High Energy Particles* (Prentice-Hall, Engelwood Cliffs, NJ, 1952).

[16] L. Landau and I. Pomerančuk, Dokl. Akad. Nauk SSSR **92**, 535 (1953); **92**, 735 (1953).

[17] A.B. Migdal, Phys. Rev. **103**, 1811 (1956); Zh. Eksp. Teor. Fiz. **32**, 633 (1957) [Sov. Phys. JETP **5**, 527 (1957)].

[18] G. Molière, Z. Naturforsch **3a**, 78 (1948).

[19] H. Snyder and W.T. Scott, Phys. Rev. **85**, 245 (1952).

[20] W.T. Scott, Phys. Rev. **76**, 220 (1949).

[21] H.A. Bethe, Phys. Rev. **89**, 1256 (1953).

[22] J.A. Wheeler and R.P. Feynman, Rev. Mod. Phys. **21**, 425 (1949).

[23] J.D. Jackson, *Classical Electrodynamics* (Wiley, New York, 1975).

[24] H.R. Allan, C.J. Crannel, J.H. Hough, P.F. Shutie, and M.P. Sun, in *Proceedings of the XIVth International Cosmic Ray Conference*, Munich, West Germany, 1975 (Max Planck Institut für Extraterrestische Physik, Garching, 1975), Vol. 8, pp. 3077–3081.

[25] J.H. Hough, J. Phys. A **6**, 892 (1973).

[26] I. Frank and I. Tamm, Dokl. Akad. Nauk SSSR **14**, 109 (1937).

[27] T. Stanev and Ch. Vankov, Comput. Phys. Commun. **16**, 363 (1979).

[28] W.R. Nelson, H. Hirayama, and D.W.O. Rogers, SLAC Report No. SLAC-265, UC-32, 1985 (unpublished).

[29] H.W. Koch and J.W. Moth, Rev. Mod. Phys. **31**, 921 (1959).

[30] E. Storm and H.I. Israel, Nucl. Data Tables **A7**, 565 (1970).

[31] T. Stanev, Ch. Vankov, R.E. Streitmatter, R.W. Ellsworth, and T. Bowen, Phys. Rev. D **25**, 1291 (1982).

[32] J.P. Ralston and D.M. McKay, in *Proceedings of the Astrophysics in Antarctica Conference*, edited by D.J. Mullan, M.A. Pomerantz, and T. Stanev, AIP Conf. Proc No. 198 (AIP, New York, 1989), p. 241; G. Smoot (private communication).

[33] K. Greisen, in *Progress of Cosmic Ray Physics*, edited by J.G. Wilson (North-Holland, Amsterdam, 1956), Vol. III, p. 1.

[34] M. Fujii and J. Nishimura, in *Proceedings of the XIth International Cosmic Ray Conference*, Budapest, Hungary, 1969, edited by T. Gémesy *et al.* (Akademiai Kiado, Budapest, 1970), pp. 709–715.

[35] M.A. Markov and I.M. Zeleznykh, Nucl. Instrum. Methods A **248**, 242 (1986).

[36] F. Halzen, E. Zas, and T. Stanev, Phys. Lett. B **257**, 432

(1991).
[37] I.N. Boldyrev, G.A. Gusev, M.A. Markov, A.L. Provorov, and I.M. Zeleznykh, in *Proceedings of the XXth International Cosmic Ray Conference*, Moscow, USSR, 1987, edited by V.A. Kozyarivsky *et al.* (Nauka, Moscow, 1987), Vol. 6, p. 472.
[38] C. Quigg, M.H. Reno, and T.P. Walker, Phys. Rev. Lett. **57**, 774 (1986).
[39] F. Halzen, J. Learned, and T. Stanev, in *Proceedings of the Antarctica Conference* [32], p. 198.